Comprehensive preparation and catalytic activities of Co/TEMPO-cellulose nanocomposites: A promising green catalyst

Nouaamane El Idrissi, Larbi Belachemi, Nicolas Merle, Philippe Zinck, Hamid Kaddami

Comprehensive preparation and catalytic activities of Co/TEMPO-Cellulose nanocomposites: A promising green catalyst

Nouaamane EL Idrissi [1,2], Larbi Belachemi[1], Nicolas Merle[2], Philippe Zinck[2], Hamid Kaddami[1, *]

1- IMED-Lab, Team of Organometallic and Macromolecular Chemistry-Composite Materials, Department of Chemical Sciences, Faculty of Science and Technology, Cadi Ayyad University Marrakech, Morocco.

2- Unité de Catalyse et Chimie du Solide, UMR 8181, Univ. Lille, CNRS, Centrale Lille, Univ. Artois, F-59650, Villeneuve d'Ascq, France

Abstract:

The present study aims to develop a green, cost effective and facile method for the production of cobalt/ 'TEMPO oxidized cellulose' (TEMPO-Cell) heterogeneous catalyst for organic chemical reactions. Indeed, 'TEMPO-Cell' was employed as solid support and stabilizing agent for the highly active cobalt metal particles via *in situ* green and facile preparation method. The process of preparation implied the reduction of cobalt precursors ($CoSO_4$) in TEMPO-Cell water dispersion in ambient conditions in the presence of $NaBH_4$ as reducing agent. It has been clearly shown that the formation of metallic cobalt particles is due to the presence of "TEMPO-CELL" which screens the Co^{2+} ions and prevents their combination with boron. The structure of the aerogel composite Co/TEMPO-Cell aerogel has been analyzed by scanning electron microscopy, energy dispersive spectroscopy, Fourier transform

infrared spectroscopy, transmission electron microscopy and X-ray photoelectron

spectrometry. These characterisations show that metallic cobalt particles have nanometric size

and are well dispersed in the ''TEMPO-CELL'' aerogel. The hybrid aerogel composites Co/

TEMPO-Cell showed excellent catalytic activity for model reactions such as the reduction of

4-nitroaniline (4-NA), 4-nitrophenol (4-NP) and 2-nitrophenol (2-NP) in water, in the

presence of $NaBH_4$. The reaction kinetic has been followed by UV-visible spectroscopy. It

was found that this catalyst is good enough to achieve 100% reduction with high reaction rate

(6 min full reaction time) and elevated turnover frequency (150 h^{-1}). The aerogel catalyst was

easily isolated from the reaction mixture by simple filtration and reused more than ten times

without significant loss of its catalytic activity.

Keywords: aerogel composite; cobalt nanoparticles; ion screening; green chemistry;

cellulose; catalysis, recyclability.

Highlights :

- ''Cobalt(0)/TEMPO oxidized cellulose'' heterogeneous catalyst was prepared.

- The characterizations have shown nanometric size and good dispersion of Co^0 particles.

- A screening effect of TEMP-Cell, which prevent Co-B components formation, was highlighted.

- High catalytic performances have been shown for the reduction of nitro to amine groups.

48 • The catalyst retains catalytic activity even after 11 cycles without significant loss of its

49 catalytic activity.

50

1. Introduction:

52 The development of green, economic and highly active catalysts is at the heart of the research

53 in catalysis. Heterogeneous catalysis is one of the most promising technology used in

54 chemical reactions and environmental remediation. [1] [2] Metal and metal oxide

55 nanoparticles (NPs) are emerging to be promising candidates due to their excellent catalytic

56 activities for different organic chemical reactions [3]. However, their applications are limited

57 because of their self-agglomeration in solution which reduces their catalytic performances. In

58 addition, they are difficult to recover from the reaction medium. This is a supplementary

59 challenge that limits their application in heterogeneous catalysis in non-supported

60 structure.[4]–[8]

61 The effective approach to overcome these problems is the immobilization of metal

62 nanoparticles on different materials. [8] In fact, supported heterogeneous catalysts is one of

63 the major focuses of research in catalysis. The supports can be Metal oxides, Silica, Zeolites,

64 Fibers, Ceramic materials, Pillared clays, and polymers notably [2]–[10]. More recently,

65 many research investigations have been directed towards the exploration of sustainable bio

66 resources to be used as support of metallic particles catalysts. Being the most abundant,

67 renewable, ecofriendly, biocompatible and biodegradable natural polymer, cellulose is widely

68 used as a biomaterial support for catalytic systems due to its properties such as high specific

69 area and strength promising good metallic nanoparticles integration. [11]–[15]

70 On the other hand, important research attention has been paid towards the utilization of the

71 first row transition metals, especially Ni, Co and Fe, as catalyst in organic synthesis. [2], [16],

72 [17] These metals represent advantageous alternative in organic synthesis compared to their

73 equivalent noble metals of the second and third rows which are less abundant and more

74 expensive. More specifically, the catalytic performances of Cobalt ions (either Co^{2+} or Co^{3+})

75 as well as the less frequently used Co^0 , have been widely and extensively studied for,

76 oxidations, C−H amination, Allylation, Alkenylation, etc. reactions. [18]–[26] Apart from the

77 organic synthesis, various cobalt oxides based supported catalysts have been explored and

78 extensively studied in high temperatures process, as active in methane catalysis

79 decomposition (CDM) for the production carbon nanomaterials, for example. This enabled to

80 reduce the CDM temperature to the range of 450–800°C [27], [28]. On the other hand, this

81 family of catalysts has been recently tested for water splitting and oxygen evolution or

82 generation [29]–[33].

83 Regarding the preparation of cobalt oxides (Co_xO_y), it worthy to emphasis that these different

84 oxides are often synthesized by high temperature processes (T>400°C) involving

85 oxidative/calcination of $Co(OH)_2$, formerly prepared by alkaline treatment of Co^{2+} salts

86 ($CoCl_2$, $CoNO_2$ or $CoSO_4$, etc.). Other investigations have been conducted on the preparation

87 of cobalt oxides by heating CO_3Co in vacuum or in CO_2, or by reduction of Co_2O_3 by NH_3 or

88 of Co_3O_4, by Carbon. *Vice versa*, Co_3O_4 can be obtained by the oxidation of CoO. [27]–[33]

89 On the other hand the preparation of metallic Co^0 from Co^{2+} ions based salts, such as $CoSO_4$,

90 can be achieved at room temperature by reduction reaction in presence of reducing agent such

91 as hydrazine [34], sodium borohydrid [35], etc.

92 In this work, we developed a novel, simple and eco-friendly biohybrid aerogels based on

93 cellulose derivative (TEMPO oxidized cellulose) as support and cobalt Metallic (Co^0)

94 particles as catalyst. The preparation of this biohybrid catalyst passes through the dispersion

95   of Co^{2+} ion salt ($CoSO_4$) in the TEMPO-cellulose aerogel and its reduction in mild condition

96   using $NaBH_4$ as reducing agent. To the best of the authors knowledge, few studies are

97   dedicated to the catalytic properties of cobalt supported on cellulose and the use of TEMPO-

98   Cellulose as catalyst support for metal nanoparticles has never been reported as far as we

99   know. In comparison to TEMPO-NFC, which production is energy demanding due to the

100   mechanical defibrillation, the use of TEMPO-cellulose is a simple and novel way to endow

101   cellulose with carboxylic groups that enhance the screen of Co^{2+} cation to permit its reduction

102   to Co^0 in presence of Borate anions. Compared to other nanocelluloses, this TEMPO-cellulose

103   can be efficient to produce stable, efficient Co^0 supported catalyst. The morphology of this

104   composite aerogel is characterized and its catalytic performances for the reduction of nitro-

105   functionalized molecules to amino-functionalized ones were tested.

106

107   **2. Material and Methods**

108   *Chemicals and starting materials:*

109   The rachis of date palm tree (*Phoenix dactylifera L.*) was used in this work as the original

110   source of cellulose. Cellulose was extracted from the rachis following the procedure well

111   described in our previous work. [36]

112   TEMPO   (1-oxo-2,2,6,6-tétraméthylpipyridine1-oxyle),   sodium   bromide,   sodium

113   hypochlorite solution (15%), HCl, NaOH, Cobalt (II) sulphate heptahydrate [$CoSO_4.7H_2O$],

114   Sodium borohydride $NaBH_4$, 4-nitroaniline (4-NA), 4-nitrophenol (4-NP) and 2-nitrophenol

115   (2-NP) were purchased from Sigma–Aldrich and used without further purification.

116   *Preparation of the TEMPO-Cell*

117   The rachis of date palm tree was used in this work as the original source of cellulose.

118   TEMPO mediated oxidation was performed following the procedure well described in our

119   previous work [37], [38]. About 2 g, *i.e.* 2.136 mmol of equivalent anhydroglucose unit

120   (AGU) of cellulose, were suspended in water (200 mL) and sonicated with a Branson Sonifier

121   for 5 min. TEMPO (32 mg, 0.065 mmol) and NaBr (0.636 g, 1.9 mmol) were added to the

122   suspension. A certain amount of the NaOCl solution, corresponding to 40.5 mL was added

123   drop wise to the cellulose suspension. The pH was adjusted at 10 by addition of a 0.1 M

124   aqueous solution of HCl. The pH of the mixture was maintained to 10 at 4 °C by continuous

125   adding of 0.1 M NaOH while stirring the suspension. After times ranging from 120 min, the

126   oxidation was terminated by adding methanol (5 mL) and the pH was adjusted to 7 by adding

127   0.1 M HCl. The concentration of carboxylic acid groups has been calculated using

128   conductimetric titration and the carboxylic content found is of 750 μmol/g; in agreement with

129   our previous results [38].

130   *Preparation of TEMPO-Cell based aerogels and catalysts*

131   Porous (Co/ TEMPO-Cell) aerogel composite was prepared by an environmentally friendly

132   method. (CoSO$_4$, 7H$_2$O) was added to a dispersion of 1wt% of TEMPO-Cell in water (the

133   amount of (CoSO$_4$, 7H$_2$O) was adjusted to obtain an aerogel composite (Co/ TEMPO-Cell)

134   with 4wt% of Cobalt metal :1g of TEMPO-Cellulose, 0.19 g of (CoSO4, 7H2O) was added).

135   Then, sodium tetrahydroboride NaBH$_4$ in distilled water was added. The amount of NaBH$_4$

136   was calculated to have a stoechiometric ratio of 6M equivalent / Co. The dispersion turns

137   immediately from pink to black colour. After that, the water was eliminated by lyophilisation

138   after freezing the dispersion at -20°C during one night. The neat TEMPO-Cell aerogel was

139   prepared lyophilisation method in the same conditions as for the supported catalyst.

140 The Co/TEMPO-Cell aerogel composite catalyst was prepared by the following reaction

141 sequences which is described in the following S1 (Supporting data S1). The first step relates

142 to the oxidation by NaOCl + NaBr + TEMPO mixture followed by treatment with cobalt

143 sulphate $CoSO_4$ in aqueous solution and reduction with $NaBH_4$ (Supporting data S1).

144

145 *Characterization techniques*

146 Infrared spectra were recorded on a FT-IR Perkin-Elmer 1000 spectrometer collecting 32

147 scans from 400 to 4000 cm^{-1}. Transmission FTIR was performed on KBr based pellets

148 prepared from grinded sample and KBr power. A separate background spectrum was collected

149 and automatically subtracted from the raw spectrum for each specimen.

150 A Philips X'per wide angle X-ray diffractometer operated at 40 kv and 30 mA with a Ni-

151 filtered CuKα radiation was used to determine the crystallinity index of the specimens. X-ray

152 diffractograms were recorded at $0.02°$ s^{-1} over a 2θ diffraction angle scan in the range 5–

153 90°. XRD was performed, especially, to check the metallic structure of Co in the aerogel.

154 The model TESCAN – VEGA3, with accelerating voltage of 12.5 kV was used. A piece of

155 aerogel was deposited on a SEM support and coated with a thin layer of carbon. EDX

156 measurement was performed using AMETEK, EDAX- OCTANE PLUS.

157 The UV–vis spectra was used to study the kinetics of the reaction of reduction 4-Nitroaniline

158 catalysed by TEMPO-Cell/Co catalyst. The spectra were taken at room temperature from 200

159 to 520 nm using a Shimadzu UV–vis spectrometer (UV-2450).

160

161 *TEM*

162

163 Transmission electron microscope FEI-Tecnai G2 operated at an accelerating voltage

7

of 200 kV was used for the morphological observation.

TEM sample was prepared by depositing two to three drops of (1 mg/1 mL) Co/TEMPO-Cellulose suspensions on carbon-coated electron microscope grids and dried at ambient temperature.

XPS

XPS analyses were performed by a Kratos Axis Ultra DLD spectrometer with monochromatized Al Kalpha X-rays operating at 180 W (12 mA and 15 kV).

Catalytic Reduction of nitro-functionalized molecules

'' An aqueous solution of 0.5 g/L NFM (nitro-functionalized molecule: 4-nitroaniline, 4-Nitrophenol or 2-Nitrophenol) is prepared, which correspond to 3,5 mM solution of NFM. For each reaction test, a 10 mL of this solution of NFM in water was used, in which an amount corresponding to 10 equivalents of $NaBH_4$ vas added. An amount of aerogel catalyst Co/TEMPO-Cell, respecting the ration N(Co)/N(NFM)=0.05 was then added. The mixture is mildly stirred at room temperature. In these condition Molar ratio of NaBH4 / NFM / Catalyst is 1000 / 100 / 5 ''.

Kinetic studies by UV-Visible spectrometry

The kinetic monitoring of the reaction by UV-Visible spectrometry requires the establishment of a calibration curve to convert the absorbance into concentration of the studied solution. Thus, we prepared solutions of NFM with different concentrations and we scanned the absorbance as a function of the wavelength (supplementary data S1-left). Monitoring the evolution of the intensity of the absorption band at 400 nm at the absorption maximum as a function of concentration allows us to obtain the calibration curve presented in S1-right. A

187 straight line obtained by the origin and which therefore verifies the law of Beer Lambert. This

188 calibration curve is used to study the kinetics of NFM reduction reaction.

189

190 **3. Results and discussion**

191 *A. Aerogels Characterization*

192 The morphology of Co/TEMPO-Cell was characterized by mean of scanning electron

193 microscopy (SEM-EDX), FTIR spectroscopy, X-ray diffraction (XRD) and XPS.

194 Figure 1 shows the SEM pictures of pure TEMPO-Cell aerogel taken as reference and those

195 of the Co/TEMPO-Cell aerogel composite with different magnifications. The optical photos

196 of the aerogels are also presented to show their macroscopic aspect (figures 1-A and 1-B).

197 The SEM micrograph of cross section of the aerogel made of pure TEMPO-Cell aerogel

198 shows the presence of micrometric fibers of 6-8 µm of diameter surrounded with films

199 (figures 1-C and 1-E). These films are certainly formed of oxidized cellulose fibrils which

200 were disintegrated from the bleached cellulose fibers during the TEMPO mediated oxidation

201 process. In fact, it's well known that TEMPO mediated oxidation of cellulose fibers

202 facilitated the dissociation of cellulose nanofibrils owing to the repulsive interactions

203 developed between the carboxylate groups created [38], [39]. These fibrils are then

204 assembled and organized as a film during the freeze-drying process. In this structure the film

205 ensure good connection and cohesion of the aerogel network which enables obtaining

206 monolith aerogel [40]. Similar structure can be observed in SEM image of Co/TEMPO-Cell

207 presented in Figures 1-H, 1-J and 1-L with the presence of small particles (diameter lower

208 than 200 nm), homogeneously dispersed in the films (Figure 1-J). These particles are certainly

209 composed of Co metal since they are absent in the pure TEMPO-Cell aerogel. The

210 observation of the Co/TEMPO-Cell aerogel at higher magnifications (figures 1-J and 1-L)

211 enabled to better distinguish these particles and to show that they are homogeneously

212 dispersed in the films of cellulose. It is worthy noticing that bigger particles (diameter up to 2

213 µm) are also observed, and they are certainly formed by the aggregation of the nanometric

214 ones.

215 EDX analyses (Figure 1- K and L) confirm that these particles are composed of cobalt. At that

216 level the type of interaction between the TEMPO-cell and the metal particle is of high

217 importance. SEM analyses cannot give information about this inquiry. However, in our

218 approach the cobalt particles are fixed and stabilized by the hydrogen bonds to the TEMPO-

219 Cell surface. It can easily be understood that the carboxylate groups at the TEMPO-Cell

220 surface play an emulsifying effect to control the size and insure good dispersion of cobalt

221 particles in the aerogel. The 2D-EDX elemental mapping enabled to show that the cobalt is

222 homogeneously distributed in the composite aerogel (supporting data S2).

A : Optic photo of pure TEMPO-Cell aerogel

B : Optic photo of Co/ TEMPO-Cell aerogel

C: Pure TEMPO-Cell aerogel : Magnification of 500
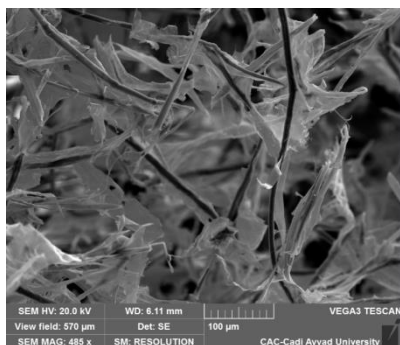
D: Co/ TEMPO-Cell aerogel : Magnification of 500
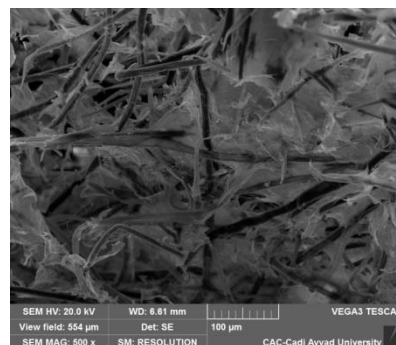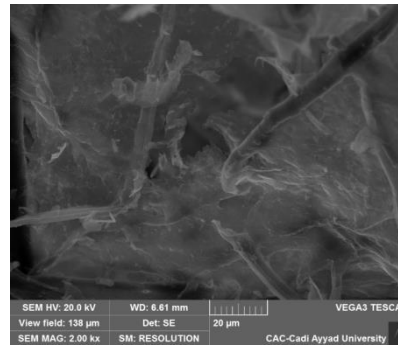

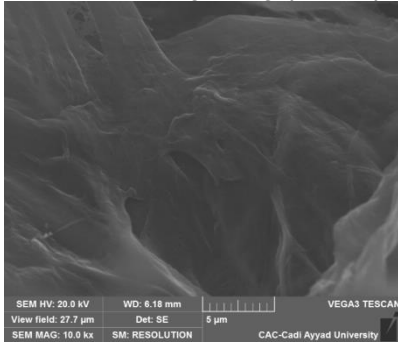*E: Pure TEMPO-Cell aerogel : Magnification of 2000*

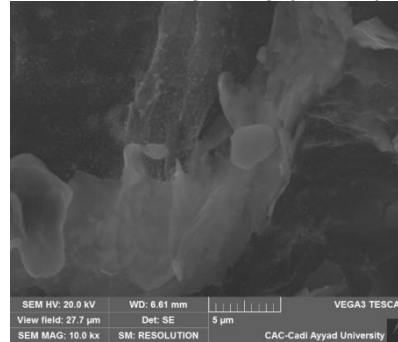*F: Co/ TEMPO-Cell aerogel : Magnification of 2000*
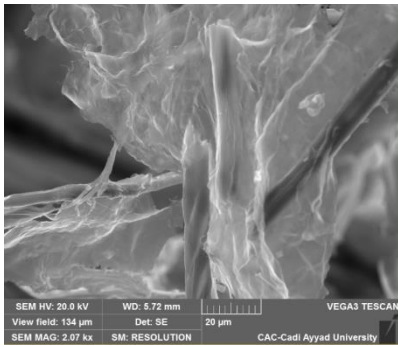
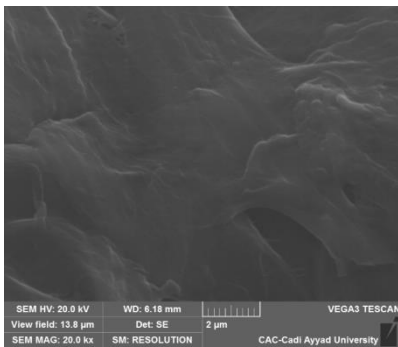G: *Pure TEMPO-Cell aerogel : Magnification of 10000*
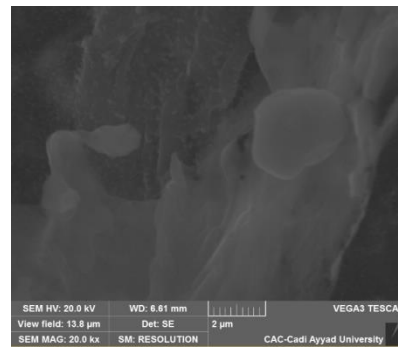

H: *Co/ TEMPO-Cell aerogel : Magnification of 10000*

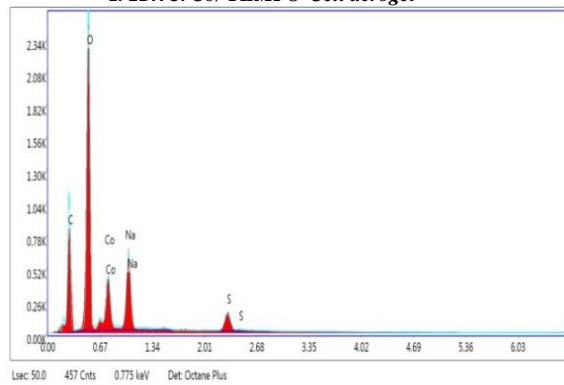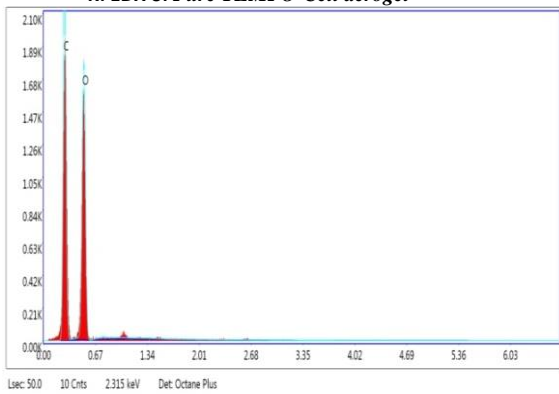I: *Pure TEMPO-Cell aerogel : Magnification of 20000*

J: *Co/ TEMPO-Cell aerogel : Magnification of 20000*

K: EDX of *Pure TEMPO-Cell aerogel*
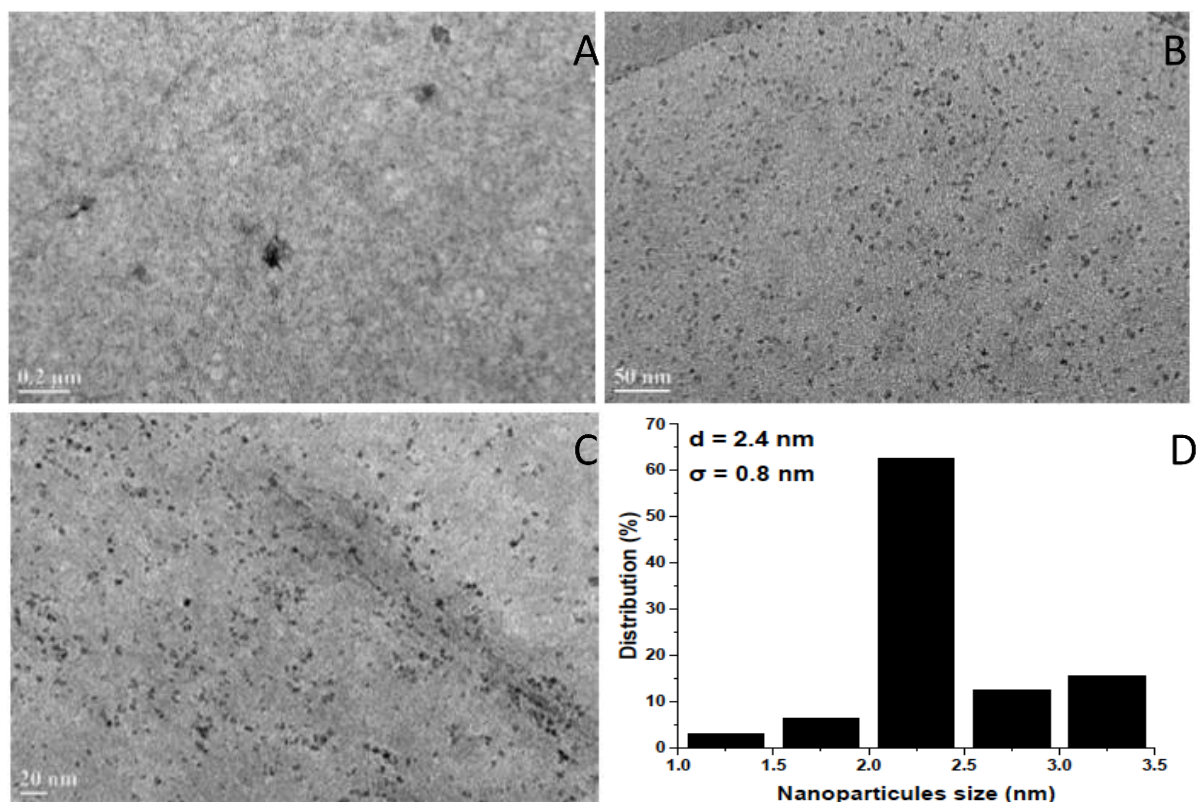

L: EDX of *Co/ TEMPO-Cell aerogel*

Figure 1: Optical, MEB and EDX characterizations of the TEMPO-Cell and Co/ TEMPO-Cell composite aerogels

11

Figure 2: TEM images of Co/ TEMPO-Cell composite aerogels and Cobalt nanoparticles diameter distribution

To have a clear idea about the formation of cobalt nanoparticles observed in the aerogels by SEM analyses, the dispersion of TEMPO oxidized cellulose supported cobalt nanoparticles was diluted in water, transferred to a carbon grid, dried in a vacuum overnight to dry and finally observed by TEM.

As shown in the Figure 2, the cobalt nanoparticles are almost less than 4 nm in diameter and are well dispersed on the whole TEMPO-cell film. Their mean diameter (d) and standard deviation (σ) were estimated to be 2.4 and 0.8 nm, respectively. These particles are very small compared to those obtained in literature (see comparison in Table 1). This shows that, in comparison to the conventional NCC and NFC nanocelluloses, the TEMPO-cell has a

12

238   pronounced emulsifying and stabilising effects, which enables the obtaining of very fine and

239   well-dispersed metallic nanoparticles.

240   **Table 1: Comparison of the metal nanoparticles size with other reported systems**

Metal	Nanoparticles size (nm)	Precursor	synthesis method	Support	Application	Reference
Au	15.6	$HAuCl_4$	reduction by NFC	NFC	Catalyst	Alle and al. [41]
Au	12-19	$HAuCl_4$	reduction by NCC	NCC	glucose detection	Alle and al. [42]
Au Ag	18-25 6-35	$HAuCl_4$, $AgNO_3$	reduction by ascorbic acid	NCC	Catalytic reduction of nitrophenol	Eisa and al. [9]
Au Pd	15-30 20	$HAuCl_4$ $PdCl_3$	reduction by dialdehyde NFC	NFC	suzuki coupling reaction	Zhang and al. [43]
Ag	10-20	$AgNO_3$	Sodium citrate	CMC/NCC	Antibacterial properties	Yunqing and al. [44]
Ag	10-100	$AgNO_3$	reduction by $NaBH_4$	NCC	sensors, catalysts, and conductive material	Dafne and al. [45]
Pd	6	$PdCl_2$	$NaBH_4$	NFC	Catalyst	Meng and a., [46]
Cu	14.65	$CuSO_4$	reduction by hydrazine	NCC	Catalytic oxidation of sulfides and alcohols	Dutta et al. [47]
Cu	7	$CuSO_4$	reduction by $NaBH_4$	NCC	C-N coupling reactions	Goswami and al. [48]
Co	**2.4**	**$CoSO_4$**	**reduction by $NaBH_4$**	**TEMPO-Cellulose**	**Catalytic reduction reactions**	**This work**

241
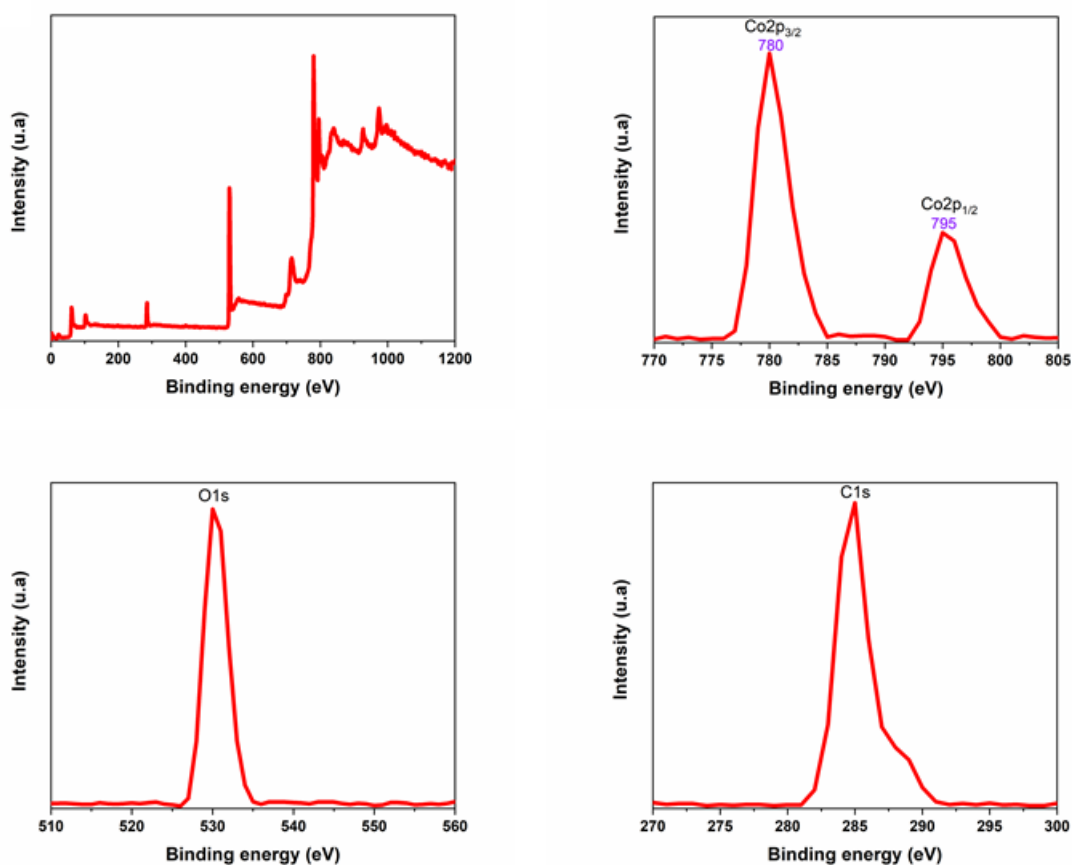
242

243

244

B
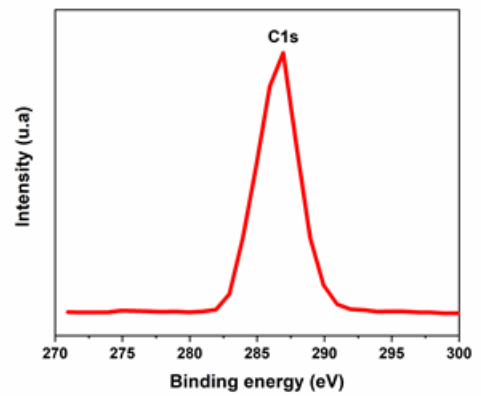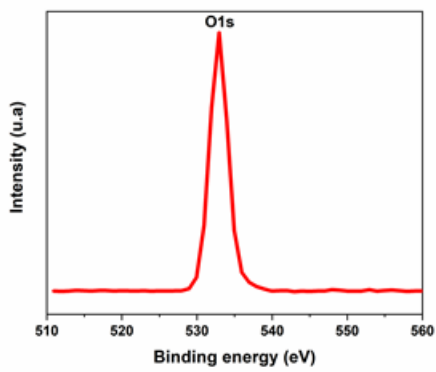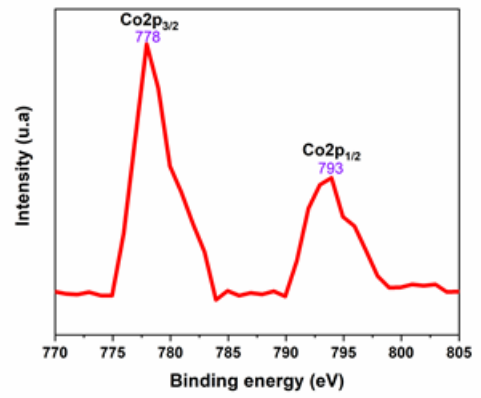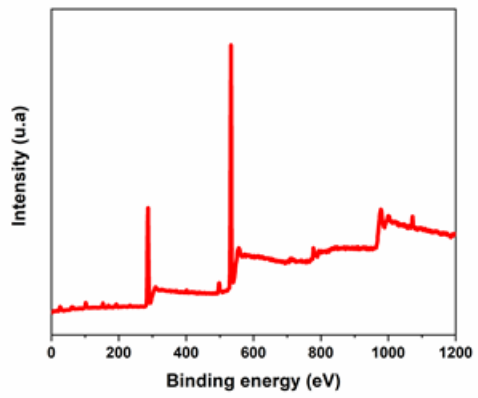
Figure 3: XPS of A: Co/TEMPO-Cell B: synthesized CoB

To ensure of the metallic structure of the observed nanoparticles, XPS analysis on the composite aerogel Co/TEMPO-Cell was performed. Figure 3-A shows the XPS spectrum obtained. The Co2p1/2 and Co2p3/2 peaks of Cellulose-TEMPO supported Cobalt nanoparticles were analyzed. Various cobalt oxidation peaks, that have been reported in the literature, [49] are 778.3 and 793.3 eV for Co^0, 780.4 and 795.8 eV for Co^{2+} and 778.5 and 794.2 eV for Co^{3+}. Accordingly, the metal nanoparticles of the studied Co/TEMPO-Cell show a Co2p3/2 base level peak at a binding energy of 778.3 eV, and Co2p1/2 at 793.3 eV, confirming the presence of the typical valence state of metallic Co^0 (Figure 3-A).

15

256 Figure 3-B shows different XPS peaks compared to the pure metal. The amorphous CoB

257 shows a peak for Co2p3/2 at 780.2 eV, which indicates that some electrons are transferred

258 from Co to B, based on their electronegativity. [50]

259

260 The FTIR spectra of the Co/TEMPO-Cell composite aerogel and the pure TEMPO-Cell

261 aerogel are presented in figure 4 and show characteristic vibration bands of the OH stretching

262 at $4000\text{--}2995\ \text{cm}^{-1}$, the OH bending of adsorbed water at 1635 or $1638\ \text{cm}^{-1}$, the CH

263 stretching at $2900\ \text{cm}^{-1}$, the HCH and OCH bending vibrations at $1430\ \text{cm}^{-1}$, the CH

264 deformation vibration at $1375\ \text{cm}^{-1}$, the stretching vibration of C=O from the free COOH

265 band near $1737\ \text{cm}^{-1}$, the C–OH bending mode at $668\ \text{cm}^{-1}$. Comparing the two spectra, it

266 observed that the stretching vibration of C=O from the free COOH band at $1737\ \text{cm}^{-1}$

267 disappears. Furthermore, the intensity of the band of C–OH bending mode at $668\ \text{cm}^{-1}$

268 strongly increases. These observations confirm that the COOH and OH groups of cellulose

269 are in interactions with cobalt nanoparticles, [51], [52].
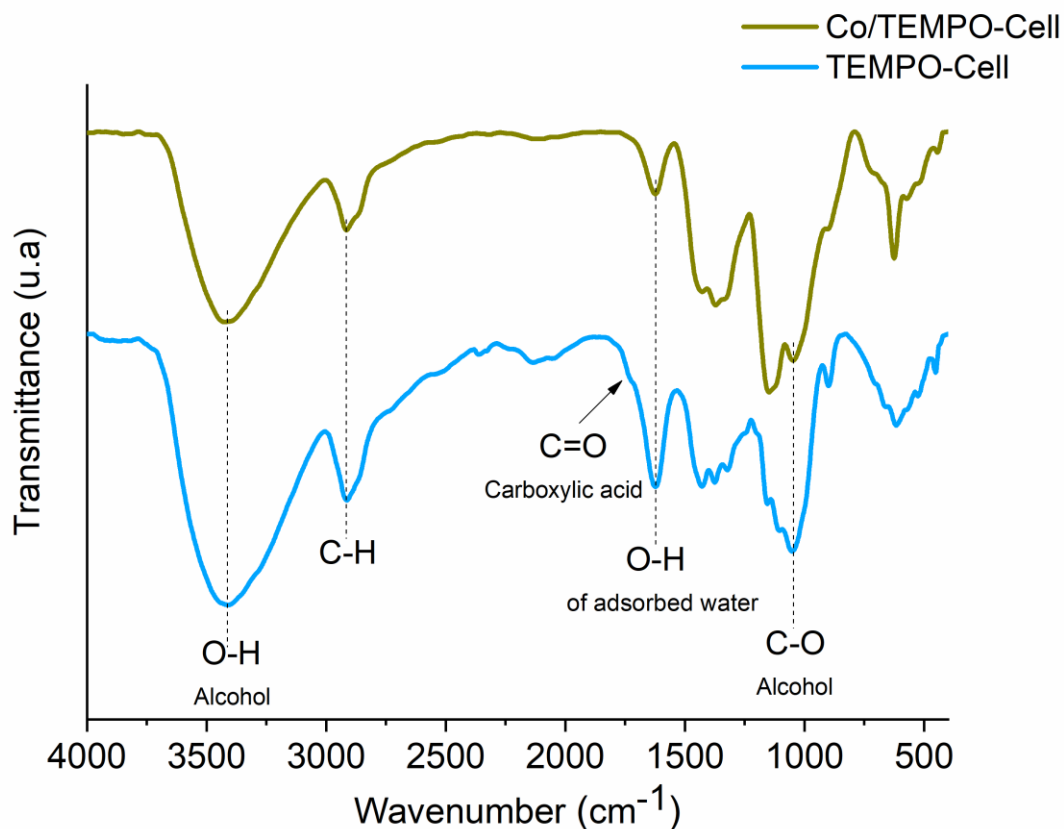
Figure 4: FTIR spectra of TEMPO-Cell and Co/ TEMPO-Cell composite aerogel.

Several reports of the literature have shown that the reduction of cobalt(II) in homogeneous media with borohydride is very complicated. [53]

To emphasis the effect of TEMPO-Cell on Co^0 metallic nanoparticle during the reduction with borohydride, a reduction of Co^{2+} ions ($CoSO_4$, $7H_2O$) in water (without TEMPO-Cell) using $NaBH_4$ in the same conditions as for the preparation of borohydride Co/TEMPO-Cell has been performed (use of sodium $NaBH_4$ in distilled water and the amount of $NaBH_4$ was calculated to have a stoichiometric ratio of 6M equivalent/Co). We reported in Figure 5-A (lower spectrum) the XRD spectra of cobalt-based powder obtained. This spectrum shows that the resulting material is amorphous since no diffraction pick could be detected. In contrast, the XRD of Co/TEMPO-Cell composite, presented in Figure 5-B (upper spectrum), shows a crystalline structure of Co^0 in its hexagonal polymorph, as indexed using Cobalt

287 According to Suraj Gupta et al. [54] and Y.D. Wang et al [55] who prepared Cobalt based

288 powder following similar procedure, this cobalt based powder is a Co-B amorphous materials.

289 The XPS analyses of this material show that the cobalt and bore metals exist in both elemental

290 and oxidized state [54]. In this structure, boron acts as the sacrificial agent in order to partially

291 protect Co from oxidation. This clearly indicates the strong interaction between Co and B in

292 CoB and Co2B boride cobalt.

293 At this stage, it's interesting to compare the reactivity of Co^{2+} toward the reductive action of

294 sodium borohydride in presence and in absence of TEMPO-oxidized cellulose. It's clear that

295 cellulose has an influence in the orientation of the catalytic reduction reaction and the

296 development of Co hexagonal metallic structure instead of Co-B and Co2B amorphous cobalt

297 borides components. It's clear that the strong interaction between B and Co in Co-B

298 component prevent the growth of crystalline structure of metallic Co (Hexagonal or Cubic

299 allomorphs). In presence TEMPO-Cell, the interactions between the hydroxyl, aldehyde and

300 carboxylate groups of TEMPO-Cell and the cobalt (II) and BH_4^- ions causes a high

301 chemoselectivity which directs the reduction reaction towards the formation of cobalt (0)

302 nanoparticles exclusively by screening the Co^{2+} ions and preventing the formation of CoB and

303 Co2B which are usually observed in this type of reduction observed in the absence of

304 TEMPO-oxidized cellulose.

305

However, it's important to emphasise that TEMPO-Cell itself is not able to reduce the Co^{2+} ions to Co^0 although it contains aldehyde and alcohol groups because of the lower value of the redox potential of the redox couple Co^{2+}/Co^0(-0.28 V) compared to that of redox couples aldehyde/alcohol (-0.2 V) and that of acid/aldehyde (-0.12 V) [56], [57] But, it clearly appears that these organic groups present in TEMPO-Cell have an important role in specifically guiding the reduction of Co^{2+} ions and the formation of Co^0 hexagonal. To this end, these hydroxyl, acid and aldehyde groups which are present at the surface of the TEMPO-oxidized cellulose matrix actively contribute to the selectivity of the catalytic reduction reaction for Co^{2+} to Co^0.

To further understand and confirm the above interpretation, hydrazine was used as reducing agent for the non-supported catalyst. The obtained metal consists of Co^0 with a cubic structure as revealed by XRD analysis presented in Fig. 5-A (upper spectrum). In fact, the XRD spectrum of the powder obtained from the reduction of $Co(SO_4)$ by hydrazine reduction shows many peaks that are related to metallic cobalt particle. All diffraction peaks were indexed using Cobalt (JCPDS: 03-056-9722) crystal phase. These peaks are compared to standard data using the High Score program which allows us to attribute the high intensity peaks observed at 2Θ= 44.57, 51.57, 75.98 and 92.66 to the plans (111), (200), (220) and (311) of cubic metal structure of cobalt. [58]
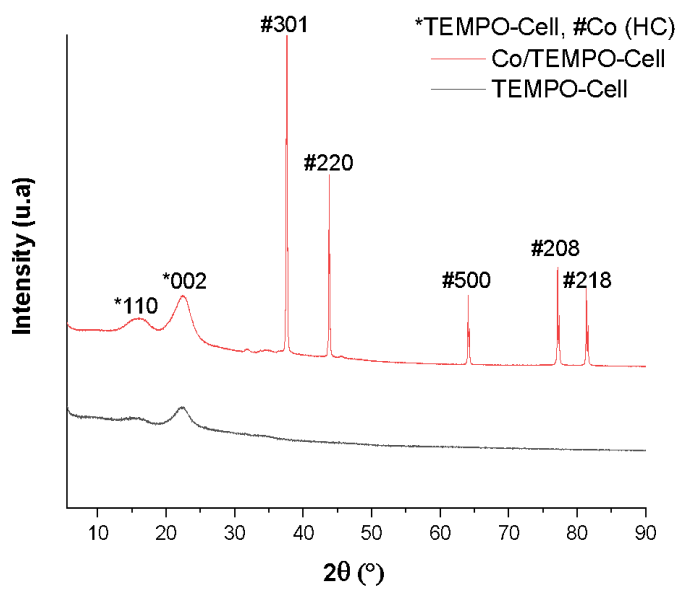
A

B
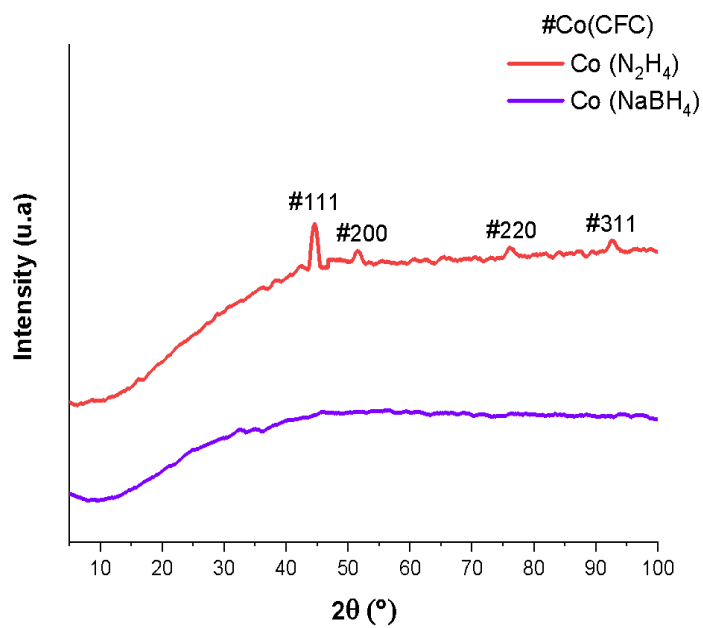
Figure 5: XRD analyses; A: XRD of the powders obtained by the reduction of CoSO$_4$ using NaBH$_4$ and Hydrazine; B : XRD spectra of the Co/TEMPO-Cell composite and TEMPO-Cell aerogels

the inducing role of the chemoselectivity of TEMPO-oxidized cellulose for the reduction reaction can be advanced from these results, which prevents the physical rapprochement and the linkage between B and Co entities, promotes the development of Co hexagonal metallic structure as indicated by DRX analyses. In fact, the TEMPO-Cell matrix represents a very important asset for controlling the reduction reaction of cobalt(II) ions and orienting it chemoselectively towards the cobalt(0) nanoparticles which are immobilized on the surface of the matrix, avoiding the formation of CoB which is much less active as a catalyst.

B. Catalytic Activity

After preparation and characterization of the composite aerogel Co/TEMPO-Cell, the catalytic activity and performances were evaluated towards the reduction in aqueous medium of 4-nitroaniline (4-NA), 4-nitrophenol (4-NP) and 2-nitrophenol (2-NP) to para-aminoaniline (4-AA), 2-aminophenol (4-AP) and 2-aminophenol (2-NP), respectively, (Supporting data S3). Para-aminoaniline is an aromatic diamine used in many application including the synthesis of Kevlar [59] and dyes matrices [60], [61], while aminophenols are biologically active and are used in the pharmaceutical industry [62].

The [Co]:[PNA]:[equivalent of NaBH$_4$] molar ratio was fixed at 5:100:1000 and the kinetics were monitored by UV–Vis absorption. The 4-NA/NaBH$_4$ solution displays a strong absorption band at 380 nm, attributed to 4-NA, which was used to follow the kinetics of the reaction.
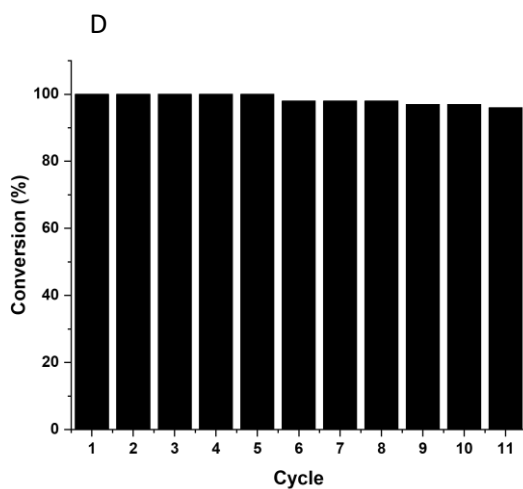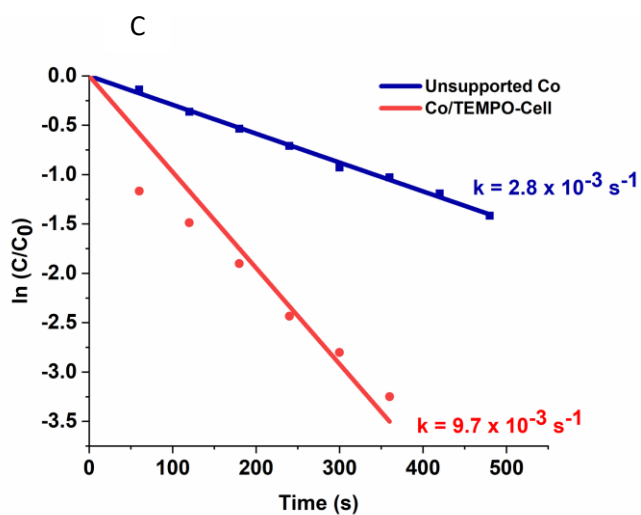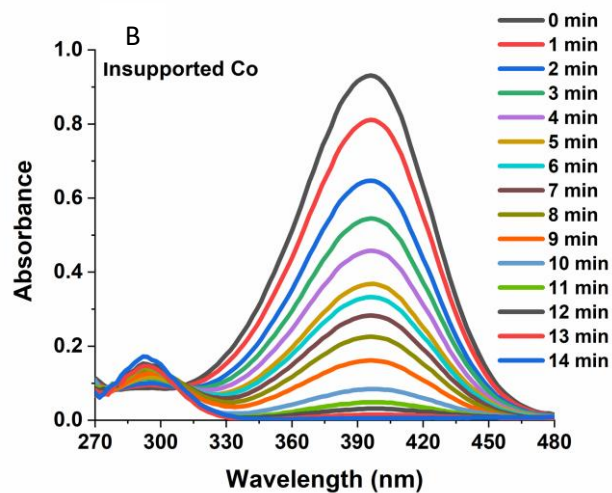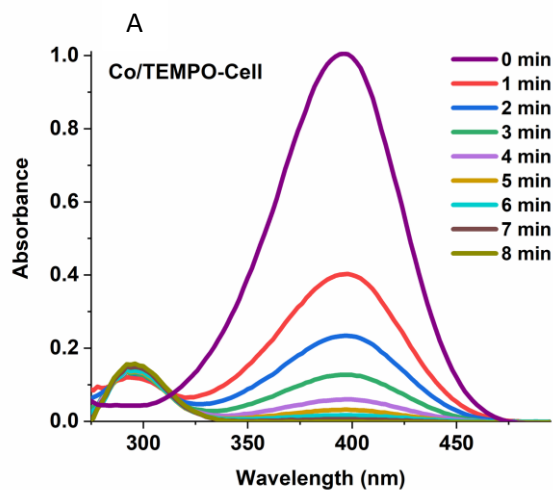
372

373

374

375

376

377

378

379

380

381

395   Figure 6: A and B : UV-Vis spectra for the reduction of 4-NA with NaBH$_4$ in aqueous

396   solution recorded every 1 min using Co/TEMPO-Cell aerogel composite and unsuported Co

397   catalysts, respectively, C: plots of ln[C$_t$/C$_0$] versus reaction time for the two reduction reaction

398   and D: results of the recyclability tests of the reduction of 4-NA with NaBH$_4$ in presence of

399   Co/TEMPO-Cellulose

400

401   The time-dependent UV–vis absorption spectra of the reaction medium during the 4-NA

402   reduction catalyzed by Co/ TEMPO-Cell composite and non-supported catalyst particle are

403   shown in Figures 6-A and 6-B. Regardless the catalyst, one can observe a reduction in the 380

404   nm absorption with time, confirming the gradual reduction of 4-NA into 4-AA. (8 min) This

405   was accompanied by the apparition and the intensity increase of a new UV absorption band at

406   302 nm attributed to 4-AA. Surprisingly, even a very low amount of supported catalyst was

407   found to be good enough to achieve 100% reduction of para-nitroaniline with a higher

408   reaction rate However, with the non-supported Co catalyst, the reaction rate is lower and the

409   reduction of 4-nitroaniline is achieved after 14 minutes (Figure 6-B).

410

411   The plot of (C$_t$/C$_0$) as a function of reaction time, where C$_0$ and C$_t$ represent the

412   concentrations at t = 0 and t of 4-NA in the reaction medium, are presented in figure 6-C

413   shows a linear relationship for the kinetics with the two catalysts (Co/TEMPO-Cell composite

414   and non-supported catalyst). This can be explained by the fact that the kinetic of this reaction

415   is governed by the reagent contact with the catalytic surface which limits the number of

416   molecules that can react at the same time.

417   The linear correlation between ln(C$_t$/C$_0$) and time at 295 °K shows that the reduction of 4-NA,

418   2-NP and 4-NP by Co/TEMPO-Cell /NaBH$_4$ follows the pseudo-first-order reaction kinetics.

419 The kinetic reaction rate constants (k_{app}) were estimated from the slope of the $\ln(C_t/C_0)$ versus

420 time liner curve. Pseudo-first order rate constant could be calculated by Langmuir–

421 Hinshelwood equation [11].

422 $\text{Ln}(C_t/C_0) = \ln(A_t/A_0) = -k \times t$

423 where, k is the rate constant. C_0 and C_t represents the initial concentration of 4-NA, 4-NP and

424 2-NP and the concentration at time t, respectively. A_0 is the initial absorbance and A_t is the

425 absorbance at any time t.

426 During the reaction, and notably in the beginning when the concentration of the substrate is

427 much higher than the concentration of the catalyst, the catalyst surface is rapidly occupied by

428 the substrate molecules and remains saturated during the reaction rending the reaction rate to

429 appear constant throughout the reduction period. From these results, the apparent rate

430 constant, k_{app}, was calculated as the slope of the linear plot of (C_t/C_0) versus time. The

431 turnover frequency (TOF, defined as the number of moles of 4-NA reduced per mole of

432 catalyst per hour) could then be evaluated from k_{app}, to compare the catalytic performances of

433 the two catalysts (Table 2). The TOF of Co/ TEMPO-Cell composite aerogel is 200 h^{-1}, while

434 that of non-supported Co catalyst is 80 h^{-1}for 4-NA (Table 2).

435 Similar trends are observed while studying the kinetic of reduction of 2-nitrophenol (2-NP)

436 and 4-nitrophenol (4-NP). The results are presented in supporting data S4 and in Table 2.

437

438

439

440

441

Table 2: Comparison of the reducing ability of Co/TEMPO-Cell aerogel composite in

reduction of nitro-functionalized molecule (NFM) with other reported systems

*CTAB : hexadecyltrimethyl ammonium bromide

** P(2-acrylamido-2- methyl-1-propansulfonic acid)–Ni nanoparticles hydrogel

Support system	Catalyst	NFM	Molar ratio of NaBH₄/NFM/Catalyst	TOF (h⁻¹)	Recyclability (number of cycles)	Reference
Graphene hydrogel	Au	4-nitrophenol	460/2,3/1	12	1	Li, Liu, and Liu [65]
Chitosan	Au	4-nitrophenol	20/6/1	50	11	Chang and Chen [66]
CNCs	Au	4-nitrophenol	9819/31,6/1	641	1	Wei Yanaand al. [67]
Poly(methyl methacrylate)	Au	4-nitrophenol	22500/15/1	89	1	Kyoko Kuroda and al. [68]
CNCs	Ag	4-nitrophenol	9/0,3/1	420	3	W. H. Eisa and al. [9]
MCC/CTAB*	Ag	4-nitrophenol	150/15/1	545	1	X. An and al. [69]
2-acrylamido-2-methyl-1-propansulfonic acid	Cu	4-nitrophenol	60000/1500/1.7	74	1	N. Sahiner and al. [70]
P(AMPS)**– hydrogel	Ni	4-nitrophenol	150/7/1	142	5	N. Sahiner and al. [71]
Cell-TEMPO	**Co**	**4-Nitroaniline**	**1000/100/5**	**200**	**11**	**This work**
Unsupported catalyst	**Co**	**4-Nitroaniline**	**1000/100/5**	**86**	**-**	**This work**
Cell-TEMPO	**Co**	**4-nitrophenol**	**1000/100/5**	**154**	**11**	**This work**
Unsupported catalyst	**Co**	**4-nitrophenol**	**1000/100/5**	**86**	**-**	**This work**
Cell-TEMPO	**Co**	**2-Nitrophenol**	**1000/100/5**	171	**11**	**This work**
Unsupported catalyst	**Co**	**2-Nitrophenol**	**1000/100/5**	**86**	**-**	**This work**

We clearly observe that the performances of Co/TEMPO-Cell composite aerogel for the

reduction reaction of nitro group are higher in comparison to non-supported catalysts. This

can be explained by the fact that the immobilization of particles on a cellulosic support

increases surface area and makes cobalt metal nanoparticles more accessible to such

nitrobenzene derivatives. The high specific area of cellulose and nanocellulose aerogels and

their composites have been widely reported in literature; it has been shown that high values

such 100 m^2/g and 200 m^2/g can be reached for these cellulosic aerogels[72-74].   Moreover,

in the case of unsupported catalyst, the aggregation and agglomeration of particles

457 significantly decreases their specific surface area, and limits their reagent accessibility.

458 Consequently, their reactivity is reduced even in the presence of an excess of $NaBH_4$. The

459 comparison of the two unsupported catalyst shows that the crystalline metallic form of cobalt

460 is more effective than unsupported catalyst for this reaction.

461 Overall, the present Co/TEMPO-Cell catalyst shows greater efficiency for the catalysis of the

462 reduction reaction of nitrobenzene derivatives when compared to previously reported systems

463 (Table 2). We conclude that the TEMPO-oxidized cellulose plays a very important role in

464 controlling the reduction reaction of cobalt(II) ions and orienting it chemo-selectively towards

465 the cobalt nanoparticles which are immobilized on the surface of the matrix. The other

466 possible reasons for the better catalytic activity could be (i) small size of the metallic cobalt

467 nanoparticles, (ii) strong interaction between metallic cobalt nanoparticles and support owing

468 to the presence of many carboxylic, aldehyde and hydroxyl groups on surface of the support

469 and (iii) the high surface area of the composite aerogels. To the best of our knowledge, the

470 present Co/TEMPO-Cell aerogel composite is an efficient catalyst for the reduction of

471 nitroaromatic compounds reported to date in comparison to other metals supported catalyst.

472 The possible mechanism for the reduction of nitrophenols and nitroaniline has been

473 previously reported. [63], [64] The complete reduction process occurs mainly on the surface

474 of metallic cobalt NPs supported on the surface of TEMPO-oxidized cellulose. In the

475 reduction of nitrophenols and nitroaniline, BH_4^- acts as donor and the nitro group act as

476 acceptor. In the first step, the nitrophenolate ion adsorbs on the surface of metallic cobalt

477 catalyst and forms active hydrogen atoms. In the reduction process, the catalytic nanoparticles

478 could act as an electronic relay system and speed up the electron transfer from BH_4^- to nitro

479 groups and the catalytic system subsequently gives aminophenols and aminoaniline. The

480 number of moles of 4-NA reduced per mole of metal catalyst per hour (turnover frequency,

481 TOF) values was 154 and 171 h^{-1} for 4-NA and 2-NP, respectively. This TOF difference

482 between 4-NP and 2-NP is most likely due to the existence of more electronic effect on 2-NP

483 which makes it relatively more ease for the substrate to be adopted on the metallic cobalt

484 nanoparticles. On the other hand, the intramolecular hydrogen bond which increases the

485 formation and adsorption of phenolate on metallic nanoparticles. The higher TOF value of 4-

486 NA 200 h^{-1} is most likely due to the high capacity of the nitrogen atom of the amino group to

487 adsorb onto nanoparticles of cobalt.

488

489 *C. Recyclability Study*

490 Recycling and reusability of heterogeneous catalysts is one of the desirable aspects in

491 commercial processes. In order to examine this issue, reusability of Co/TEMPO-Cell aerogel

492 composite was examined towards $NaBH_4$ reduction of the three nitrophenol derivatives (4-

493 NA, 4-NP and 2-NP). After completion of the reactions, the composite catalyst was separated

494 from the reaction mixture by simple filtration, washed with EtOH and then dried under air

495 atmosphere for additional using at the next runs. The obtained results show that Co/TEMPO-

496 Cell aerogel composite was reused for 11 consecutive cycles without significant loss of its

497 catalytic activity (Figure 6-D) for the reduction of 4-NA and in supporting data S4 for the

498 reduction of 4-NP and 2-NP.

499

500

501

504 **4. Conclusion**

505 In this study, Co/TEMPO-Cellulose aerogel composite was prepared by simple *insitu*

506 reduction of Co^{2+} ($CoSO_4$) in water dispersion of TEMPO oxidized-Cell using sodium

507 borohydride $NaBH_4$ as reducing agent. The *in situ* reduction process in the presence of

508 TEMPO oxidized-cellulose very selectively oriented the reduction reaction for the metallic

509 particles Co^0 in the presence of $NaBH_4$ as reducing agent. With this reduction process, the

510 formation of CoB and Co2B is not observed, and Co metal nanoparticles were formed

511 exclusively. The catalytic activity and recyclability of this composite aerogel catalyst were

512 studied and compared with non-supported Co metal particles. The structure of Co/TEMPO-

513 Cell aerogel composites were investigated by means of MEB microscopy, FTIR and DRX and

514 XPS. These analyses confirm the excellent dispersion of the Co nanoparticles in the aerogel

515 matrix which is controlled by their interactions with cellulose functional groups (COOH,

516 CHO and OH groups) on its surface. The catalytic performances of Co/TEMPO-Cell aerogel

517 composites and non-supported Cobalt particles were compared by measuring the turnover

518 frequency (TOF) obtained after catalytic reduction of three nitroarenes as model reactions.

519 Compared to non-supported Co particles, the catalytic activity of Co/TEMPO-Cell aerogel

520 composites was significantly higher (High TOF and high reaction kinetic for the aerogel

521 composite versus low TOF and low reaction kinetic for the unsupported Co). The

522 recyclability of the aerogel composite was established; the aerogel composite retains good

523 catalytic activity even after 11 cycles without significant loss of its catalytic activity. The

524 efficient catalytic activity of the Co/TEMPO-Cell aerogel composite may be attributed to

525 accessible, well-dispersed, and active metallic cobalt nanoparticles present on the TEMPO-

526 oxidized cellulose support. In this way, sustainability demands, including those associated

527 with environmental, economic and remediation issues can be addressed by the proposed

528 concept.

529

531

Reference:

[1]   P. Munnik, P. E. De Jongh, and K. P. De Jong, "Recent Developments in the Synthesis of Supported Catalysts," *Chem. Rev.*, vol. 115, no. 14, pp. 6687–6718, Jul. 2015, doi: 10.1021/CR500486U.

[2]   A. Mondal, A. Mondal, B. Adhikary, and D. K. Mukherjee, "Cobalt nanoparticles as reusable catalysts for reduction of 4-nitrophenol under mild conditions," *Bull. Mater. Sci.*, vol. 40, no. 2, pp. 321–328, Apr. 2017, doi: 10.1007/S12034-017-1367-3.

[3]   G. C. Y. Choo, H. Miyamura, and S. Kobayashi, "Synergistic cascade catalysis by metal nanoparticles and Lewis acids in hydrogen autotransfer," *Chem. Sci.*, vol. 6, no. 3, pp. 1719–1727, Mar. 2015, doi: 10.1039/C4SC03627A.

[4]   P. Mondal, A. Sinha, N. Salam, A. S. Roy, N. R. Jana, and S. M. Islam, "Enhanced catalytic performance by copper nanoparticle–graphene based composite," *RSC Adv.*, vol. 3, no. 16, pp. 5615–5623, Mar. 2013, doi: 10.1039/C3RA23280H.

[5]   R. García-Álvarez, A. E. Díaz-Álvarez, P. Crochet, and V. Cadierno, "Ruthenium-catalyzed one-pot synthesis of primary amides from aldehydes in water," *RSC Adv.*, vol. 3, no. 17, pp. 5889–5894, Apr. 2013, doi: 10.1039/C3RA23195J.

[6]   M. Hu, J. Sen Jiang, F. X. Bu, X. L. Cheng, C. C. Lin, and Y. Zeng, "Hierarchical magnetic iron (III) oxides prepared by solid-state thermal decomposition of coordination polymers," *RSC Adv.*, vol. 2, no. 11, pp. 4782–4786, Jun. 2012, doi: 10.1039/C2RA01190E/.

[7]   Y. W. C. Cao, R. Jin, and C. A. Mirkin, "Nanoparticles with Raman spectroscopic fingerprints for DNA and RNA detection," *Science*, vol. 297, no. 5586, pp. 1536–1540, Aug. 2002, doi: 10.1126/SCIENCE.297.5586.1536.

[8]   M. Kaushik and A. Moores, "Review: Nanocelluloses as versatile supports for metal nanoparticles and applications in catalysis," *Green Chem.*, vol. 18, no. 3, pp. 622–637, 2016, doi: 10.1039/C5GC02500A.

[9]   W. H. Eisa, A. M. Abdelgawad, and O. J. Rojas, "Solid-State Synthesis of Metal Nanoparticles Supported on Cellulose Nanocrystals and Their Catalytic Activity," *ACS Sustain. Chem. Eng.*, vol. 6, no. 3, pp. 3974–3983, 2018, doi: 10.1021/acssuschemeng.7b04333.

[10]   P. Munnik, P. E. De Jongh, and K. P. De Jong, "Recent Developments in the Synthesis of Supported Catalysts," *Chem. Rev.*, vol. 115, no. 14, pp. 6687–6718, 2015, doi: 10.1021/cr500486u.

[11]   M. Gopiraman, D. Deng, S. Saravanamoorthy, I. M. Chung, and I. S. Kim, "Gold, silver and nickel nanoparticle anchored cellulose nanofiber composites as highly active catalysts for the rapid and selective reduction of nitrophenols in water," *RSC Adv.*, vol. 8, no. 6, pp. 3014–3023, Jan. 2018, doi: 10.1039/C7RA10489H.

[12]   J. Gu, C. Hu, W. Zhang, and A. B. Dichiara, "Reagentless preparation of shape memory cellulose nanofibril aerogels decorated with Pd nanoparticles and their application in dye discoloration," *Appl. Catal. B Environ.*, vol. 237, pp. 482–490, Dec.

588   2018, doi: 10.1016/J.APCATB.2018.06.002.

589   [13]   M. Nasrollahzadeh, N. Shafiei, Z. Nezafat, N. S. Soheili Bidgoli, and F. Soleimani,
590   "Recent progresses in the application of cellulose, starch, alginate, gum, pectin, chitin
591   and chitosan based (nano)catalysts in sustainable and selective oxidation reactions: A
592   review," *Carbohydr. Polym.*, vol. 241, p. 116353, Aug. 2020, doi:
593   10.1016/J.CARBPOL.2020.116353.

594   [14]   S. Jeremic *et al.*, "Production of bacterial nanocellulose (BNC) and its application as a
595   solid support in transition metal catalysed cross-coupling reactions," *Int. J. Biol.*
596   *Macromol.*, vol. 129, pp. 351–360, May 2019, doi: 10.1016/J.IJBIOMAC.2019.01.154.

597   [15]   Q. Zhang, L. Zhang, W. Wu, and H. Xiao, "Methods and applications of nanocellulose
598   loaded with inorganic nanomaterials: A review," *Carbohydr. Polym.*, vol. 229, p.
599   115454, Feb. 2020, doi: 10.1016/J.CARBPOL.2019.115454.

600   [16]   N. Rajesh, N. Barsu, and B. Sundararaju, "Recent advances in C(sp3)H bond
601   carbonylation by first row transition metals," *Tetrahedron Lett.*, vol. 59, no. 10, pp.
602   862–868, Mar. 2018, doi: 10.1016/J.TETLET.2018.01.065.

603   [17]   A. Singh and L. Spiccia, "Water oxidation catalysts based on abundant 1st row
604   transition metals," *Coord. Chem. Rev.*, vol. 257, no. 17–18, pp. 2607–2622, Sep. 2013,
605   doi: 10.1016/J.CCR.2013.02.027.

606   [18]   P. Hu and M. Long, "Cobalt-catalyzed sulfate radical-based advanced oxidation: A
607   review on heterogeneous catalysts and applications," *Appl. Catal. B Environ.*, vol. 181,
608   pp. 103–117, Feb. 2016, doi: 10.1016/J.APCATB.2015.07.024.

609   [19]   S. Dey and G. C. Dhal, "The catalytic activity of cobalt nanoparticles for low-
610   temperature oxidation of carbon monoxide," *Mater. Today Chem.*, vol. 14, p. 100198,
611   Dec. 2019, doi: 10.1016/J.MTCHEM.2019.100198.

612   [20]   B. Sun, T. Yoshino, S. Matsunaga, and M. Kanai, "Air-Stable
613   Carbonyl(pentamethylcyclopentadienyl)cobalt Diiodide Complex as a Precursor for
614   Cationic (Pentamethylcyclopentadienyl)cobalt(III) Catalysis: Application for Directed
615   C-2 Selective C?H Amidation of Indoles," *Adv. Synth.*
616   *Catal.*, vol. 356, no. 7, pp. 1491–1495, May 2014, doi: 10.1002/ADSC.201301110.

617   [21]   S. Prakash, R. Kuppusamy, and C. H. Cheng, "Cobalt-Catalyzed Annulation Reactions
618   via C−H Bond Activation," *ChemCatChem*, vol. 10, no. 4, pp. 683–705, Feb. 2018,
619   doi: 10.1002/CCTC.201701559.

620   [22]   Y. Park, Y. Kim, and S. Chang, "Transition Metal-Catalyzed C–H Amination: Scope,
621   Mechanism, and Applications," *Chem. Rev.*, vol. 117, no. 13, pp. 9247–9301, Jul.
622   2017, doi: 10.1021/ACS.CHEMREV.6B00644.

623   [23]   X. Jiang *et al.*, "Cobalt(III)-catalyzed fast and solvent-free C-H allylation of indoles
624   using mechanochemistry," *J. Org. Chem.*, vol. 82, no. 19, pp. 10665–10672, Oct. 2017,
625   doi: 10.1021/ACS.JOC.7B01695/SUPPL_FILE/JO7B01695_SI_001.PDF.

626   [24]   K. Sakata, M. Eda, Y. Kitaoka, T. Yoshino, and S. Matsunaga, "Cp∗CoIII-Catalyzed
627   C-H Alkenylation/Annulation Reactions of Indoles with Alkynes: A DFT Study," *J.*
628   *Org. Chem.*, vol. 82, no. 14, pp. 7379–7387, Jul. 2017, doi:
629   10.1021/ACS.JOC.7B01047/SUPPL_FILE/JO7B01047_SI_001.PDF.

630 [25] P. G. Chirila and C. J. Whiteoak, "Recent advances using [Cp*Co(CO)I2] catalysts as a
631   powerful tool for C–H functionalisation," *Dalt. Trans.*, vol. 46, no. 30, pp. 9721–9739,
632   Aug. 2017, doi: 10.1039/C7DT01980G.

633 [26] Y. Kommagalla and N. Chatani, "Cobalt(II)-catalyzed CH functionalization using an
634   N,N′-bidentate directing group," *Coord. Chem. Rev.*, vol. 350, pp. 117–135, Nov. 2017,
635   doi: 10.1016/J.CCR.2017.06.018.

636 [27] J. Majewska and B. Michalkiewicz, "Low temperature one-step synthesis of cobalt
637   nanowires encapsulated in carbon," *Appl. Phys. A Mater. Sci. Process.*, vol. 111, no. 4,
638   pp. 1013–1016, Jun. 2013, doi: 10.1007/S00339-013-7698-Z/FIGURES/4.

639 [28] M. Pudukudy and Z. Yaakob, "Methane decomposition over Ni, Co and Fe based
640   monometallic catalysts supported on sol gel derived SiO2 microflakes," *Chem. Eng. J.*,
641   vol. 262, pp. 1009–1021, Feb. 2015, doi: 10.1016/J.CEJ.2014.10.077.

642 [29] Y. C. Liu, J. A. Koza, and J. A. Switzer, "Conversion of electrodeposited Co(OH)2 to
643   CoOOH and Co3O4, and comparison of their catalytic activity for the oxygen
644   evolution reaction," *Electrochim. Acta*, vol. 140, pp. 359–365, Sep. 2014, doi:
645   10.1016/J.ELECTACTA.2014.04.036.

646 [30] J. Wang *et al.*, "Synergistic effect of two actions sites on cobalt oxides towards
647   electrochemical water-oxidation," *Nano Energy*, vol. 42, pp. 98–105, Dec. 2017, doi:
648   10.1016/J.NANOEN.2017.10.044.

649 [31] Y. P. Zhu, T. Y. Ma, M. Jaroniec, and S. Z. Qiao, " Self-Templating Synthesis of
650   Hollow Co 3 O 4 Microtube Arrays for Highly Efficient Water Electrolysis ," *Angew.
651   Chemie*, vol. 129, no. 5, pp. 1344–1348, Jan. 2017, doi: 10.1002/ANGE.201610413.

652 [32] X. Yang *et al.*, "Highly acid-durable carbon coated Co3O4 nanoarrays as efficient
653   oxygen evolution electrocatalysts," *Nano Energy*, vol. 25, pp. 42–50, Jul. 2016, doi:
654   10.1016/J.NANOEN.2016.04.035.

655 [33] Y. Dou *et al.*, "Graphene-like holey Co3O4 nanosheets as a highly efficient catalyst for
656   oxygen evolution reaction," *Nano Energy*, vol. 30, pp. 267–275, Dec. 2016, doi:
657   10.1016/J.NANOEN.2016.10.020.

658 [34] H. Zhao, J. Hao, Y. Ban, Y. Sha, H. Zhou, and Q. Liu, "Novel and efficient cobalt
659   catalysts synthesized by one-step solution phase reduction for the conversion of
660   biomass derived ethyl levulinate," *Catal. Today*, vol. 319, pp. 145–154, Jan. 2019, doi:
661   10.1016/J.CATTOD.2018.08.011.

662 [35] D. Wang, J. Zhou, J. Li, X. Jiang, Y. Wang, and F. Gao, "Cobalt-boron nanoparticles
663   anchored on graphene as anode of lithium ion batteries," *Chem. Eng. J.*, vol. 360, pp.
664   271–279, Mar. 2019, doi: 10.1016/J.CEJ.2018.11.238.

665 [36] A. Bendahou, Y. Habibi, H. Kaddami, and A. Dufresne, "Physico-chemical
666   characterization of palm from Phoenix Dactylifera-L, preparation of cellulose whiskers
667   and natural rubber-based nanocomposites," *J. Biobased Mater. Bioenergy*, vol. 3, no. 1,
668   pp. 81–90, 2009, doi: 10.1166/JBMB.2009.1011.

669 [37] A. Sbiai, H. Kaddami, H. Sautereau, A. Maazouz, and E. Fleury, "TEMPO-mediated
670   oxidation of lignocellulosic fibers from date palm leaves," *Carbohydr. Polym.*, vol. 86,
671   no. 4, pp. 1445–1450, Oct. 2011, doi: 10.1016/J.CARBPOL.2011.06.005.

[38] K. Benhamou, A. Dufresne, A. Magnin, G. Mortha, and H. Kaddami, "Control of size and viscoelastic properties of nanofibrillated cellulose from palm tree by varying the TEMPO-mediated oxidation time," *Carbohydr. Polym.*, vol. 99, pp. 74–83, Jan. 2014, doi: 10.1016/J.CARBPOL.2013.08.032.

[39] T. Saito *et al.*, "Individualization of Nano-Sized Plant Cellulose Fibrils by Direct Surface Carboxylation Using TEMPO Catalyst under Neutral Conditions," *Biomacromolecules*, vol. 10, no. 7, pp. 1992–1996, Jul. 2009, doi: 10.1021/BM900414T.

[40] D. Bendahou, A. Bendahou, B. Seantier, Y. Grohens, and H. Kaddami, "Nano-fibrillated cellulose-zeolites based new hybrid composites aerogels with super thermal insulating properties," *Ind. Crops Prod.*, vol. 65, pp. 374–382, Mar. 2015, doi: 10.1016/J.INDCROP.2014.11.012.

[41] M. Alle, S. C. Park, R. Bandi, S. H. Lee, and J. C. Kim, "Rapid in-situ growth of gold nanoparticles on cationic cellulose nanofibrils: Recyclable nanozyme for the colorimetric glucose detection," *Carbohydr. Polym.*, vol. 253, no. July 2020, p. 117239, 2021, doi: 10.1016/j.carbpol.2020.117239.

[42] M. Alle, R. Bandi, G. Sharma, S. H. Lee, and J. C. Kim, "Shape recoverable, Au nanoparticles loaded nanocellulose foams as a recyclable catalyst for the dynamic and batch discoloration of dyes," *Carbohydr. Polym.*, vol. 258, no. November 2020, p. 117693, 2021, doi: 10.1016/j.carbpol.2021.117693.

[43] K. Zhang, M. Shen, H. Liu, S. Shang, D. Wang, and H. Liimatainen, "Facile synthesis of palladium and gold nanoparticles by using dialdehyde nanocellulose as template and reducing agent," *Carbohydr. Polym.*, vol. 186, pp. 132–139, Apr. 2018, doi: 10.1016/J.CARBPOL.2018.01.048.

[44] Y. He, H. Li, X. Fei, and L. Peng, "Carboxymethyl cellulose/cellulose nanocrystals immobilized silver nanoparticles as an effective coating to improve barrier and antibacterial properties of paper for food packaging applications," *Carbohydr. Polym.*, vol. 252, no. September, p. 117156, 2021, doi: 10.1016/j.carbpol.2020.117156.

[45] D. Musino, C. Rivard, G. Landrot, B. Novales, T. Rabilloud, and I. Capron, "Hydroxyl groups on cellulose nanocrystal surfaces form nucleation points for silver nanoparticles of varying shapes and sizes," *J. Colloid Interface Sci.*, vol. 584, pp. 360–371, 2021, doi: 10.1016/j.jcis.2020.09.082.

[46] J. Meng, Y. Liu, X. Shi, W. Chen, X. Zhang, and H. Yu, "Recyclable nanocellulose-confined palladium nanoparticles with enhanced room-temperature catalytic activity and chemoselectivity," *Sci. China Mater.*, vol. 64, no. 3, pp. 621–630, 2021, doi: 10.1007/s40843-020-1438-9.

[47] A. Dutta *et al.*, "Copper Nanoparticles Immobilized on Nanocellulose: A Novel and Efficient Heterogeneous Catalyst for Controlled and Selective Oxidation of Sulfides and Alcohols," *Catal. Letters*, vol. 149, no. 1, pp. 141–150, 2019, doi: 10.1007/s10562-018-2615-x.

[48] M. Goswami and A. M. Das, "Synthesis of cellulose impregnated copper nanoparticles as an efficient heterogeneous catalyst for C–N coupling reactions under mild

714 conditions," *Carbohydr. Polym.*, vol. 195, no. April, pp. 189–198, 2018, doi:
715 10.1016/j.carbpol.2018.04.033.

[49] M. Z. Rong, M. Q. Zhang, H. B. Wang, and H. M. Zeng, "Surface modification of
717 magnetic metal nanoparticles through irradiation graft polymerization," *Appl. Surf.*
718 *Sci.*, vol. 200, no. 1–4, pp. 76–93, Nov. 2002, doi: 10.1016/S0169-4332(02)00620-7.

[50] X. Li *et al.*, "Hybridization of inorganic CoB noncrystal with graphene and its Kubas-
720 enhanced hydrogen," *RSC Adv.*, vol. 6, no. December 2017, pp. 93238–93244, 2016,
721 doi: 10.1039/C6RA19238F.

[51] S. Karami, B. Zeynizadeh, and Z. Shokri, "Cellulose supported bimetallic Fe–Cu
723 nanoparticles: a magnetically recoverable nanocatalyst for quick reduction of
724 nitroarenes to amines in water," *Cellul. 2018 256*, vol. 25, no. 6, pp. 3295–3305, Apr.
725 2018, doi: 10.1007/S10570-018-1809-0.

[52] H. Heidari, "Ag Nanoparticle/Nanofibrillated Cellulose Composite as an Effective and
727 Green Catalyst for Reduction of 4-Nitrophenol," *J. Clust. Sci. 2018 293*, vol. 29, no. 3,
728 pp. 475–481, Feb. 2018, doi: 10.1007/S10876-018-1351-0.

[53] J. Lu, D. B. Dreisinger, and W. C. Cooper, "Cobalt precipitation by reduction with
730 sodium borohydride," *Hydrometallurgy*, vol. 45, no. 3, pp. 305–322, Jul. 1997, doi:
731 10.1016/S0304-386X(96)00086-2.

[54] S. Gupta, N. Patel, A. Miotello, and D. C. Kothari, "Cobalt-Boride: An efficient and
733 robust electrocatalyst for Hydrogen Evolution Reaction," *J. Power Sources*, vol. 279,
734 pp. 620–625, Apr. 2015, doi: 10.1016/J.JPOWSOUR.2015.01.009.

[55] Y. D. Wang, X. P. Ai, Y. L. Cao, and H. X. Yang, "Exceptional electrochemical
736 activities of amorphous Fe–B and Co–B alloy powders used as high capacity anode
737 materials," *Electrochem. commun.*, vol. 6, no. 8, pp. 780–784, Aug. 2004, doi:
738 10.1016/J.ELECOM.2004.06.002.

[56] "CRC Handbook of Chemistry and Physics, 88th ed Editor-in-Chief: David R. Lide
740 (National Institute of Standards and Technology) CRC Press/Taylor & Francis Group:
741 Boca Raton, FL. 2007. 2640 pp. $139.95. ISBN 0-8493-0488-1.," *J. Am. Chem. Soc.*,
742 vol. 130, no. 1, pp. 382–382, Jan. 2007, doi: 10.1021/JA077011D.

[57] "CRC Handbook of Chemistry and Physics, 91st Edition - كتب Google."
744 https://books.google.fr/books?id=oROqPwAACAAJ&dq=CRC+Handbook+of+Chemi
745 stry+and+Physics,+91th&hl=ar&sa=X&redir_esc=y (accessed Nov. 21, 2021).

[58] S. S. Djokić, "Electroless Deposition of Cobalt Using Hydrazine as a Reducing Agent,"
747 *J. Electrochem. Soc.*, vol. 144, no. 7, pp. 2358–2363, Jul. 1997, doi:
748 10.1149/1.1837818/XML.

[59] P. Finocchiaro *et al.*, "Synthesis and characterization of novel polyamides from new
750 aromatic phosphonate diamine monomer," *Eur. Polym. J.*, vol. 44, no. 8, pp. 2639–
751 2651, Aug. 2008, doi: 10.1016/J.EURPOLYMJ.2008.05.022.

[60] H. Park *et al.*, "Skin irritation and sensitization potential of oxidative hair dye
753 substances evaluated with in vitro, in chemico and in silico test methods," *Food Chem.*
754 *Toxicol.*, vol. 121, pp. 360–366, Nov. 2018, doi: 10.1016/J.FCT.2018.09.017.

[61] S. Dayan, N. Kayaci, and N. Kalaycioğlu Özpozan, "Improved performance with

756 molecular design of Ruthenium(II) complexes bearing diamine-based bidentate ligands
757 as sensitizer for dye-sensitized solar cells (DSSC)," *J. Mol. Struct.*, vol. 1209, p.
758 127920, Jun. 2020, doi: 10.1016/J.MOLSTRUC.2020.127920.

759 [62] S. C. Mitchell and R. H. Waring, "Aminophenols," *Ullmann's Encycl. Ind. Chem.*, Sep.
760 2000, doi: 10.1002/14356007.A02_099.

761 [63] B. Naik, S. Hazra, V. S. Prasad, and N. N. Ghosh, "Short Communication," *Catal.*
762 *Commun.*, vol. 12, no. 12, pp. 1104–1108, Jul. 2011, doi:
763 10.1016/J.CATCOM.2011.03.028.

764 [64] J. Liu *et al.*, "A thermosensitive hydrogel carrier for nickel nanoparticles," *Colloids*
765 *Interface Sci. Commun.*, vol. 4, pp. 1–4, Jan. 2015, doi:
766 10.1016/J.COLCOM.2014.12.001.

767 [65] J. Li, C. Y. Liu, and Y. Liu, "Au/graphene hydrogel: Synthesis, characterization and its
768 use for catalytic reduction of 4-nitrophenol," *J. Mater. Chem.*, vol. 22, no. 17, pp.
769 8426–8430, 2012, doi: 10.1039/c2jm16386a.

770 [66] Y. C. Chang and D. H. Chen, "Catalytic reduction of 4-nitrophenol by magnetically
771 recoverable Au nanocatalyst," *J. Hazard. Mater.*, vol. 165, no. 1–3, pp. 664–669, 2009,
772 doi: 10.1016/j.jhazmat.2008.10.034.

773 [67] W. Yan *et al.*, "Facile and green synthesis of cellulose nanocrystal-supported gold
774 nanoparticles with superior catalytic activity," *Carbohydr. Polym.*, vol. 140, pp. 66–73,
775 2016, doi: 10.1016/j.carbpol.2015.12.049.

776 [68] K. Kuroda, T. Ishida, and M. Haruta, "Reduction of 4-nitrophenol to 4-aminophenol
777 over Au nanoparticles deposited on PMMA," *J. Mol. Catal. A Chem.*, vol. 298, no. 1–
778 2, pp. 7–11, 2009, doi: 10.1016/j.molcata.2008.09.009.

779 [69] X. An, Y. Long, and Y. Ni, "Cellulose nanocrystal/hexadecyltrimethylammonium
780 bromide/silver nanoparticle composite as a catalyst for reduction of 4-nitrophenol,"
781 *Carbohydr. Polym.*, vol. 156, pp. 253–258, 2017, doi: 10.1016/j.carbpol.2016.08.099.

782 [70] N. Sahiner, "Soft and flexible hydrogel templates of different sizes and various
783 functionalities for metal nanoparticle preparation and their use in catalysis," *Prog.*
784 *Polym. Sci.*, vol. 38, no. 9, pp. 1329–1356, 2013, doi:
785 10.1016/j.progpolymsci.2013.06.004.

786 [71] N. Sahiner, H. Ozay, O. Ozay, and N. Aktas, "New catalytic route: Hydrogels as
787 templates and reactors for in situ Ni nanoparticle synthesis and usage in the reduction
788 of 2- and 4-nitrophenols," *Appl. Catal. A Gen.*, vol. 385, no. 1–2, pp. 201–207, 2010,
789 doi: 10.1016/j.apcata.2010.07.004.

790 Teresa Cristina Fonseca Silva et al. Cellulose (2012) 19:1945–1956,

791 Dounia Bendahou et al. Industrial Crops and Products, 65, 2015, 374-382,

792 Houssine Sehaqui etComposites Science and Technology, 71 (13), 2011, 1593-1599)

793

794

815   **Table 2:** Comparison of the reducing ability of Co/TEMPO-Cell aerogel composite in

816   reduction of nitro-functionalized molecule (NFM) with other reported systems

817

818